Time Characteristics of the Imaging Quality Degradation Caused by Aero-Optical Effects Under Hypersonic Conditions

Lin Ju, Zhigang Fan, Bo Liu, Yue Ming, Xiaotian Shi, and Xueshen Li

***Abstract*—In this study, the time characteristics of the image quality degradation caused by aero-optical effects in time-varying hypersonic conditions have been investigated to ensure the precision of the guidance capability. The time-accurate imaging scheme based on time discretization has been used to predict the imaging quality of the infrared detection system caused by aero-optical effects. Using wave aberration, point spread function, and peak signal-to-noise ratio as imaging evaluation indicators, the time characteristics of the image quality degradation caused by aero-optical effects under hypersonic conditions have been obtained. During the working process, the image quality degradation caused by the aero-optical transmission effect is not obvious, and limited influence mainly comes from the aero-optical transmission effect of the flow field. With time marching, the aero-thermal radiation effect will rapidly degrade the image quality. The influence of the aero-thermal radiation predominantly determines the image deterioration.**

***Index Terms*—Aero-optical effects, hypersonic conditions, infrared dome, aero-optical transmission effects, aero-thermal radiation effects.**

I. Introduction

INFRARED detection technology has become the main detection method for precision-guided weapons due to its advantages of high guidance accuracy, strong anti-interference ability, and all-weather work [1]. With the development of modern warfare, the requirement of faster speed of infrared precision-guided weapons has become increasingly important. However, this will bring new challenges to infrared detection technology. Infrared detection technology is required to identify and track targets under hypersonic conditions accurately. When the infrared detection system is in a working state, the hypersonic condition causes the fluid structure surrounding the optical windows to continuously undergo complex evolution in a short period, while the temperature of the optical window evolves accordingly [2], [3]. Further, both of these evolutions will cause variations in the index of refraction and cause the refractive index of the fluid and optical window to be in a non-uniform gradient state. The target signal passes through the time-varying refractive index field, the obtained target image looks blurry, has jitter, and faces energy attenuation. This is called the aero-optical transmission effect. At the same time, the optical window will be rapidly heated to a high temperature in hypersonic conditions. The heated optical window will radiate strong rays outward. These rays will be received by the infrared detector and will cause serious interference to the real rays of the actual target, leading the image obtained by the infrared detection system to have background noise [4], [5], [6]. This is the aero-thermal radiation effects. The aero-optical transmission effects and the aero-thermal radiation effects are collectively referred to as aero-optical effects. Aero-optical effects will lead to a serious imaging quality degradation of the infrared detection system, which has time-varying characteristics, affecting its ability to identify, track and strike targets. In hypersonic conditions, the infrared detection system needs to ensure good imaging quality at all times to capture target information in real time. Hence, studying the time characteristics on the degradation of image quality caused by aero-optical effects under hypersonic conditions is crucial to ensure the precise guidance capability of the infrared detection system.

Currently, significant research efforts are being taken on understanding the aero-optical effect. In the supersonic mixing layer, Wang et al. studied the image deterioration attributed to the aero-optical effects [7]. Chen et al. investigated the effect of the aero-optical transmission of a faceted dome on the deterioration of the imaging quality [4]. Wang et al. studied how an airborne infrared detection system was influenced by the aero-thermal radiation of the optical dome that was heated aerodynamically [8]. In the case of an airborne IR-optical system, Liu et al. investigated the joint aero-optical transmission effect of the optical window (aerodynamically heated) and the aerodynamic flow field (non-uniform) on the imaging quality [9]. Wang et al. studied the influence of the flight conditions on the deterioration of the dome imaging quality owing to the aero-optical effects [6]. A study on the overall aero-optical effect should include the thermal radiation achieved by the optical window as well as the aero-optical transmission achieved collectively by the optical window and the fluid. Based on the results from previous studies, it can be understood that the current image quality degradation

Manuscript received 6 September 2022; accepted 8 September 2022. Date of publication 13 September 2022; date of current version 22 September 2022. *(Corresponding author: Lin Ju.)*

Lin Ju and Bo Liu are with the Key Laboratory of Science and Technology on Space Optoelectronic Precision Measurement, Institute of Optics and Electronics, Chinese Academy of Sciences, Sichuan, Chengdu 610042, China (e-mail: littlejxl@126.com; boliu@ioe.ac.cn).

Zhigang Fan, Yue Ming, Xiaotian Shi, and Xueshen Li are with the Research Center of Space Optical Engineering, Harbin Institute of Technology, Heilongjiang, Harbin 150001, China (e-mail: fzg@hit.edu.cn; 2668223030@qq.com; 690709894@qq.com; 402074489@qq.com).

Digital Object Identifier 10.1109/JPHOT.2022.3206224

This work is licensed under a Creative Commons Attribution 4.0 License. For more information, see https://creativecommons.org/licenses/by/4.0/

research focuses only on a certain aspect of the aero-optical performance. As a result, it is difficult to accurately predict the impact of aviation optical effects on image quality degradation. Hence, a comprehensive study for the impact of aero-optical effects is essential.

Further, in a hypersonic condition, the time-varying characteristics of fluid and optical window evolution cannot be ignored. The fluid and optical windows' physical parameters are operated at a noticeably smaller time scale than thermal evolution. The influence of fluid evolution and structural evolution on the image quality degradation of infrared detection systems is different at different time scales. In the process of studying the influence of aero-optical effects on the degradation of image quality, the coupling relationship between the fluid and the optical window and the time-varying characteristics of the evolution cannot be ignored. However, although there are currently some related studies on aero-optical effects, they almost ignore the coupling relationship between the fluid and the optical window and their time-varying characteristics. Thus, it is difficult to realize the imaging quality prediction for the infrared detection system in the real working state. Hence, when studying the time characteristics of the imaging quality degradation caused by aero-optical effects, it is necessary to consider the coupling relationship between the fluid and the optical window and its time-varying characteristics. In this study, the numerical simulation calculation model corresponding to the prediction scheme considers the progress of time-accuracy imaging and includes the coupling relationship between the fluid and the optical window.

Researchers have also carried out studies on image quality degradation factors caused by aerodynamic effects. Xu and Cai explored the influence of flight altitude on the deviation of fluid aero-optical imaging [10], [11]. Gordeyev et al. studied the influence of the fluid density, Mach number, and azimuth on the optical distortion caused by the aero-optical transmission effect [12], [13], [14]. Xiao and Fan et al. studied the influence of different shapes of the optical windows on the aero-optical effect exerted by the optical window combined with the flow field [15], [16]. To the best of our knowledge, the time-varying characteristics of hypersonic conditions are ignored, and no study has been done on time characteristics of the imaging quality degradation caused by aero-optical effects. As a result, the time-varying imaging state of the infrared detection system cannot be accurately evaluated during the entire working process under hypersonic conditions. Hence, a study for time characteristics of the imaging quality degradation caused by aero-optical effects under hypersonic conditions is essential.

In this study, the time-accurate joint aero-optical effect prediction scheme and the numerical simulation calculation model of imaging quality prediction based on time discretization have been developed. Then, evaluation indicators have been proposed for evaluating the imaging quality of the infrared detection system. Finally, the developed prediction scheme and the simulation model have been used for predicting the image quality caused by the aero-optical effect over time. The influencing laws of the aero-optical effect on the imaging quality and its time characteristics have been derived. In particular, this study takes into account the aero-optical effect of the flow field and the optical window in addition to the aero-thermal radiation effect of the optical window, and the full impact of aero-optical effects has been analyzed.

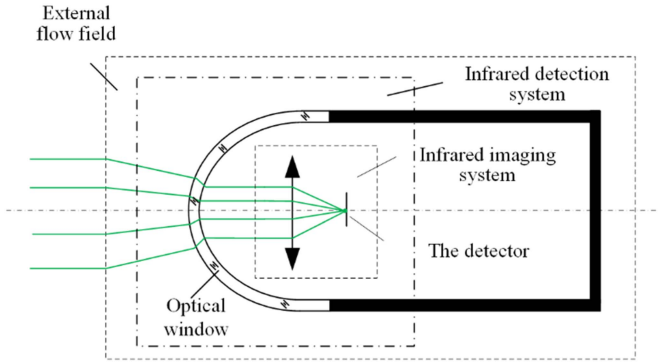

Fig. 1. Schematic showing the transmission of radiation through the optical window.

II. The Time-Accurate Joint Aero-Optical Effect Prediction Scheme

A. Model for the Aero-Optical Transmission Effect

An infrared detection system needs to complete target recognition under hypersonic conditions in which its external flow field forms a variety of complex fluid structures, such as strong turbulence boundary layers and shock layers. The density of fluids having various complex structures exhibits uneven gradient changes. This causes the refractive index of the external flow field to have a non-uniform gradient distribution state [3], [7], [17]. Furthermore, the optical window is located at the forefront of the infrared detection system and is directly exposed to the hypersonic fluid environment. As the optical window is heated by the aerodynamic heat flow, its temperature will rise rapidly. Due to the non-uniform aerodynamic heating of the optical window by the fluid, parameters of the optical window such as stress, temperature, deformation, and strain present a non-uniform distribution state [4], [6], [15]. Under the influence of the elasto- and thermo-optical effects, the refractive index of the optical window also exhibits a non-uniform gradient distribution. During transmission of the original infrared signal of the target via the refractive index field (gradient, non-uniform) of the external flow field and the optical window, its phase will be added, and the beam wavefront undergoes distortion. Fig. 1 depicts the propagation of a target infrared signal under the influence of the aero-optical effect.

Under hypersonic conditions, the fluid and structural physics parameters are operated at a noticeably smaller time scale compared to thermal evolution. In addition, the influence of fluid evolution and structural evolution on the aero-optical transmission properties is different at different time scales. Hence, time marching is required to capture the time records at a small time scale, which encapsulates the longer time scale. In this paper, based on the generation mechanism of the aero-optical effect, a time-accurate aero-optical transmission effect prediction scheme based on time-discreteness has been developed.

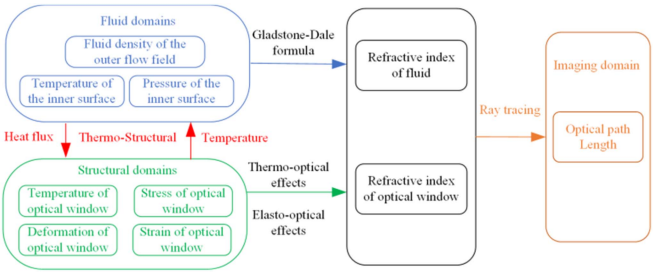

Fig. 2. Schematic showing the time-accurate aero-optical transmission effect prediction.

In particular, the coupling relationship with time variation between fluid and structure has been considered in this scheme. The specific scheme is shown in Fig. 2.

Fluid domain calculations need to acquire the general density in the external flow field, the temperature, pressure, and the heat flux of the inner surface of the external flow field. The refractive index field is calculated using the external flow field density, whereas the other results are used as the boundary conditions for the heat transfer calculation of the structure. Complete the coupling calculation between the flow field and the structure field. The structural domain calculation obtains the temperature, deformation, stress, and strain due to the high temperature of the optical window. Among them, the temperature, stress, and strain results use the thermo-optical effect and the elasto-optical effect to calculate the refractive index field of the optical window. In the imaging domain, ray tracing is used to track the target signal to obtain the optical path length (OPL) of the signal to the infrared imaging system.

The fluid, structural, and thermal fields are all governed by the equations of continuity of mass, momentum, and energy. The compressible Navier-Stokes (N-S) equations constitute the basic equations for solving the fluid motion [18], [19], [20]. Using the second-order backward Euler equation to discretize the fluid domain in terms of time [21], [22], [23]. Choosing the Crank-Nicolson scheme to discretize the heat transfer domain in terms of time [24]. The Newmark-β method is used to discretize the domains in terms of time [25], [26]. In accordance with Fermat's principle, the optical path of the target signal to the infrared detection system is obtained [6].

The refractive index in the external flow field depends on its density. Using the Gladstone-Dale formula, the refractive index in the flow field can be written as

$$N = 1 + K_{\mathrm{GD}}\rho \tag{1}$$

and

$$K_{\mathrm{GD}}(\lambda) = 2.23 \times 10^{-4}\left(1 + \frac{7.52 \times 10^{-3}}{\lambda^2}\right) \tag{2}$$

where N represents the refractive index, ρ represents the density value of the fluid and λ denotes the wavelength.

The changes in the refractive index in the optical window could arise due to the elasto- and thermo-optical effects. The thermo-optical effect has a stronger influence on the changes in the refractive index as compared to the elasto-optical effect. In this study, the impact of only the thermo-optical effect has been taken into account. Thus, the refractive index changes in the optical material with temperature can be defined as the thermo-optical effect.

$$n[\lambda, t(x,y,z)] = n(\lambda, t_0) + \frac{\mathrm{d}(\lambda, t)}{\mathrm{d}t}\Delta t(x,y,z) \tag{3}$$

where $n(\lambda, t_0)$ represents the refractive index at a reference temperature t_0 at an arbitrary grid node, $\mathrm{d}\,n(\lambda,t)/\mathrm{d}\,t$ represents the thermo-optical coefficient, and$\Delta t(x,y,z)$ represents the change in the temperature $t(x,y,z)$ with respect to t_0.

After obtaining the refractive index field of the flow field and the optical window, the infrared signal transmitted in the non-uniform gradient refractive index field needs to be traced. For the same, the optical path of the infrared signal to the exit pupil of the infrared system needs to be calculated. In accordance with Fermat's principle, the light equation is given by

$$\frac{\mathrm{d}}{\mathrm{d}\,s}\left[n(r)\frac{\mathrm{d}\,r}{\mathrm{d}\,s}\right] = \nabla n(r) \tag{4}$$

where r represents the position vector corresponding to the ray propagation, $\mathrm{d}s$ represents the step length of the transmission path, and $n(r)$ represents the distribution of the refractive index values. The fourth-order Runge-Kutta method was employed for solving the Fermat formula. The coordinates at the signal propagation point are given by

$$\begin{cases} \boldsymbol{r}_{i+1} = \boldsymbol{r}_i + \frac{h}{6}(\boldsymbol{K}_1 + 2\boldsymbol{K}_2 + 2\boldsymbol{K}_3 + \boldsymbol{K}_4) \\ \boldsymbol{T}_{i+1} = \boldsymbol{T}_i + \frac{h}{6}(\boldsymbol{L}_1 + 2\boldsymbol{L}_2 + 2\boldsymbol{L}_3 + \boldsymbol{L}_4) \end{cases} \tag{5}$$

where

$$\begin{cases} \frac{\mathrm{d}\boldsymbol{r}}{\mathrm{d}p} = \boldsymbol{T} \\ \frac{\mathrm{d}\boldsymbol{T}}{dp} = n\nabla n \end{cases} \tag{6}$$

where $p = \int \frac{\mathrm{d}s}{n}$.

The coefficients can be expressed as

$$\begin{cases} K_1 = T_i \\ K_2 = T_i + hL_1/2 \\ K_3 = T_i + hL_2/2 \\ K_4 = T_i + hL_3 \end{cases} \tag{7}$$

where

$$\begin{cases} L_1 = n(r)\nabla n(r)(atr_i) \\ L_2 = n(r)\nabla n(r)\,(atr_i + hK_1/2, \text{in the direction of } K_1) \\ L_3 = n(r)\nabla n(r)\,(atr_i + hK_2/2, \text{in the direction of } K_2) \\ L_4 = n(r)\nabla n(r)\,(atr_i + hK_3, \text{in the direction of } K_3) \end{cases} \tag{8}$$

When the signal is at the ith step of ray tracing, the optical path length (OPL) is given by

$$\mathrm{OPL}_i = \int_{t_0}^{t_0+\Delta t}\left(N_i\frac{\partial l_i}{\partial t} + l_i\frac{\partial N_i}{\partial t}\right)\mathrm{d}t + \int_{\varepsilon_0}^{\varepsilon_0+\Delta\varepsilon}\left(N_i\frac{\partial l_i}{\partial \varepsilon} + l_i\frac{\partial N_i}{\partial \varepsilon}\right)\mathrm{d}\varepsilon \tag{9}$$

where l is the signal transmission distance.

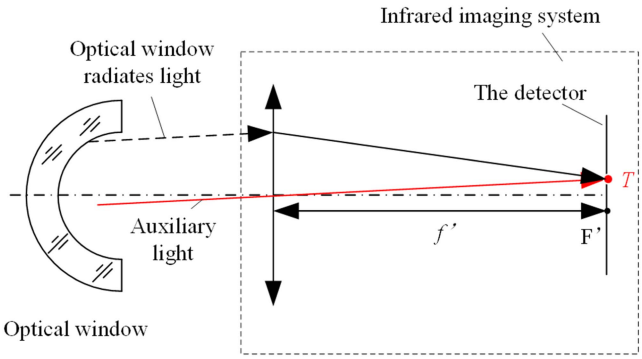

Fig. 3. Schematic showing the radiation transmission through the optical window.

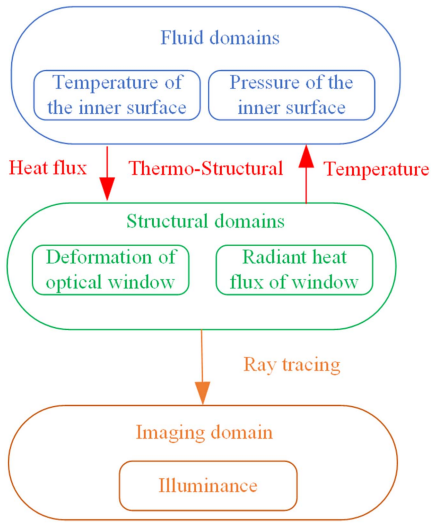

Fig. 4. Schematic showing the time-accurate aero-thermal radiation effect prediction.

B. Model for Aero-Thermal Radiation Effects

In a hypersonic condition, the heating of the optical window to a high temperature will lead to the emission of a large amount of infrared radiation, which is nothing but the aero-thermal radiation effect. In the calculation of thermal radiation illuminance, the optical window is not only a medium for signal transmission but also a radiation source [6], [8]. A schematic showing the radiation transmission is given in Fig. 3.

In this study, a time-accurate aero-thermal radiation effect prediction scheme based on time-discreteness has been developed. The specific scheme is shown in Fig. 4. The radiant heat flow results are used for calculating the energy of the infrared radiation rays. The ray is radiated from the optical window by tracing to obtain the irradiance reaching the detector surface in the imaging domain.

The fourth-order Runge-Kutta method is also used for ray tracing in thermal radiation calculations. According to the radiation law, the panel radiance, L_λ, can be expressed as

$$L_\lambda = \frac{2\varepsilon h v_c^2 \lambda^{-5}}{\exp\left(h v_c / k T_i \lambda\right) - 1} \tag{10}$$

where ε is the surface element emission rate, h is the Planck constant, v_c is the velocity of light in the medium, k is the Boltzmann constant, and λ is the wavelength.

Every radiation surface element is a Lambert radiator that has identical radiant luminance along each direction. The radiation rays are traced by ray tracing. The amount of light received by the detector pixels and the energy are measured to calculate the irradiance on the detector surface. Suppose that the infrared radiated ray direction forms an angle relative to the normal of surface element whose area is ds, then the radiation power of the infrared rays arising from the surface element at a spatial angle and in a waveband can be expressed as [27]

$$\mathrm{d}\, W = L_\lambda \cos\theta \,\mathrm{d}\lambda \,\mathrm{d}\, s \,\mathrm{d}\,\Omega \tag{11}$$

The irradiance on the detector surface is thus calculated using the above equation.

III. Image Quality Evaluation Index Model

In this study, three parameters, namely, the wave aberration and the point spread function (PSF), have been combined with the peak signal-to-noise ratio (PSNR) for evaluating the imaging quality of an infrared detection system.

A. The Wave Aberration

Using the OPL obtained by ray tracing, the wave aberration, W_j, of the exit pupil is calculated as follows:

$$\begin{aligned} \mathrm{OPL}_0 &= \frac{1}{N_r} \sum_j \mathrm{OPL}_j \\ W_j(x, y) &= \frac{2\pi}{\lambda} \left(\mathrm{OPL}_j - \mathrm{OPL}_0\right) \end{aligned} \tag{12}$$

where N_r is the number of rays, and x, y are the coordinates of the exit pupil position.

B. The Point Spread Function

The PSF, i.e., PSF(x', y') , is calculated from the pupil function that is expressed as

$$A(x', y') = \begin{cases} a(x, y) \exp\left[jW(x, y)\right] & x^2 + y^2 \le (D/2)^2 \\ 0 & x^2 + y^2 \ge (D/2)^2 \end{cases} \tag{13}$$

where $a(x, y)$ denotes the amplitude distribution followed by the pupil function, and D represents the diameter of the pupil.

For a supersonic aircraft, its course of target imaging conforms to the requirement of far-field approximation in most cases. Following the Huygens' principle, the amplitude distribution of the light field on the image plane is calculated by taking a Fourier transform as follows [27]:

$$U(x', y') = \iint A(x, y) \exp\left[-j \frac{2\pi}{\lambda f} \left(x x' + y y'\right)\right] \mathrm{d}\, x \mathrm{d}\, y \tag{14}$$

Given the proportionality of the light intensity to the amplitude square, the PFS can be calculated as

$$\mathrm{PSF}(x', y') = \left|U(x', y')\right|^2 = U(x', y')\, U^*(x', y') \tag{15}$$

TABLE I
OPERATING PARAMETERS USED FOR THE INFRARED DETECTION SYSTEM IN THE SIMULATION

Working condition parameters	Value
Simulated height	10 km
Simulate high speed	As shown in Fig. 5
Simulation time	15 s
Simulated angle of attack	0°

C. The Peak Signal-to-Noise Ratio

Based on the optical dome radiation power, the output voltage of every pixel of the detector was calculated using the following equation:

$$V_{ij} = G \cdot R_{ij} \cdot \mathrm{d}W + V_{Nij} \tag{16}$$

where V_{ij} represents the output voltage related to the radiation power at pixel (i, j), G represents the gain of the preamplifier of the detector, R_{ij} represents the response rate at pixel (i, j), $\mathrm{d}W$ represents the radiation power associated with the optical dome, and V_{Nij} represents the root mean square noise at pixel (i, j). The output voltage can be transferred to the gray value via the preprocessing circuit, and thus a distorted image is obtained owing to the interference of the thermal radiation from the optical dome.

The distorted image quality was assessed by the most objective and common parameter, namely, the peak signal-to-noise ratio (PSNR), which is given by [28]

$$\mathrm{PSNR}(f, G) = 10 \log 10 \left[\frac{(M-1)^2}{\mathrm{MSE}(f, G)} \right] \tag{17}$$

where M denotes the number of pixels in the image and MSE is the mean squared error of the images.

IV. TIME CHARACTERISTICS OF THE IMAGING QUALITY DEGRADATION

Currently, an infrared detection system with a spherical optical window is one of the most widely used target tracking devices. Hence, in this study, an infrared-guided weapon equipped with a spherical optical window has been chosen as the prediction object, and the law of imaging quality degradation in an infrared detection system as a function of its increasing working time has been studied. The simulation performed in this study used air-to-air missiles as the research background. During the working of an air-to-air missile, its flight speed changes with time, which needs to be considered in the simulation, whereas the change in its altitude and angle of attack can be ignored. The operating parameters of the infrared detection system used in this simulation are given in Table I. The flight speed of the missile as a function of time is shown in Fig. 5.

The parameters of the infrared detection system are shown in Table II.

The uneven gradient refractive index field is a direct contributor to the phenomenon of aero-optical transmission. In addition, the radiation illuminance received by the detector is the direct cause of the aero-thermal radiation effect. Hence, this paper discusses the refractive index of the external flow field and the optical window, and the detector's irradiance.

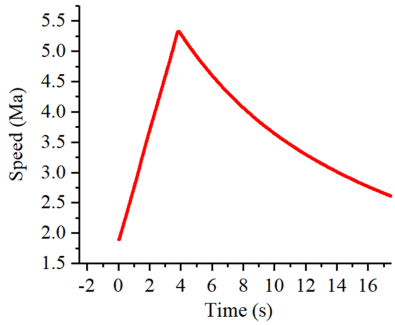

Fig. 5. Flight speed of an air-to-air-missile as a function of time.

TABLE II
PARAMETERS OF THE INFRARED DETECTION SYSTEM OF THE INFRARED DETECTION SYSTEM

Infrared detection system parameters	Value
Bottom diameter	160 mm
Wavelength	4.2 μm
Diameters of the entrance pupil	120 mm
Detector pixels length	30 μm×30 μm
Number of detector pixels	256 × 256

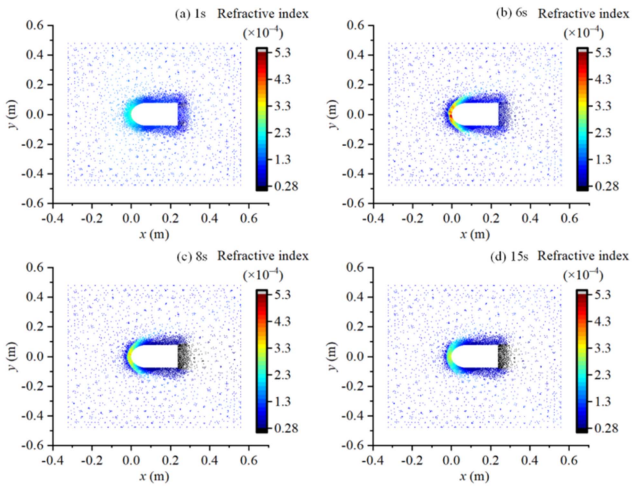

Fig. 6. Refractive index distribution in the hypersonic external flow.

The distribution of the change in the refractive index in the hypersonic external flow has been shown in Fig. 6 from which the change in the refractive index of different fluid structure states can be clearly observed. The refractive index of the fluid turbulence layer and the shock layer changes drastically and becomes a non-uniform gradient distribution state. In addition, as the working time progresses, the refractive index changes relatively sharply when $t < 6$ s and tends to be stable after $t > 8$ s.

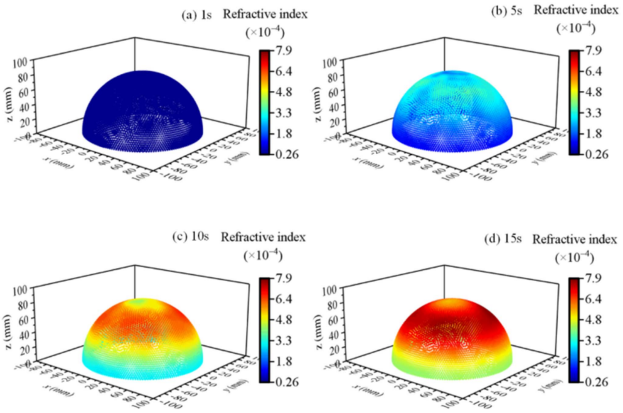

Fig. 7. Refractive index distribution related to the optical window.

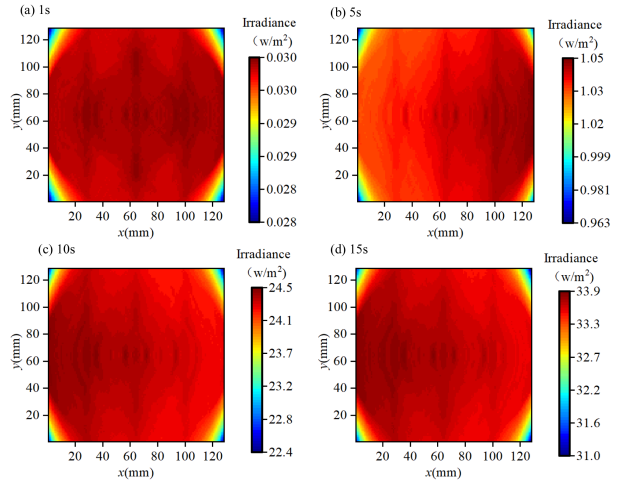

Fig. 8. Irradiance received by the detector surface.

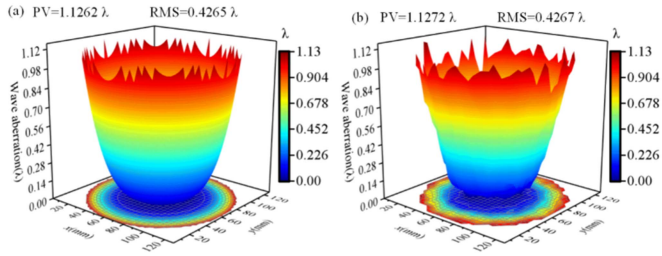

Fig. 9. Results of the wave aberration introduced by the optical window itself. (a) Shows the results obtained using the Zemax software, whereas (b) Shows the result obtained using the indigenously developed software.

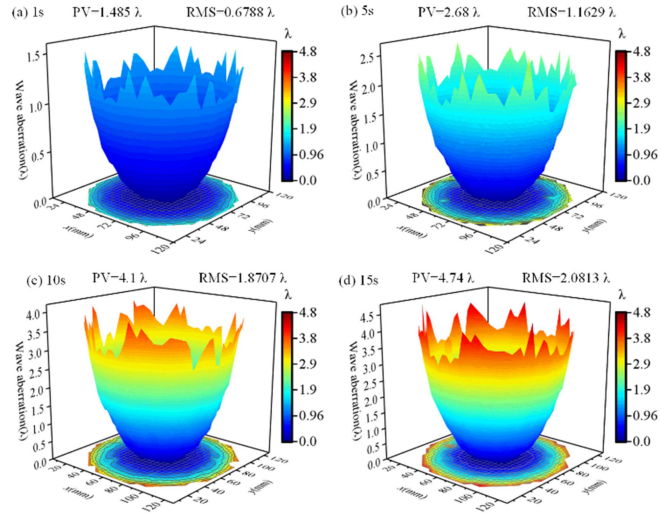

Fig. 10. Wave aberration resulting due to the joint aero-optical transmission effect.

The distribution of the change in the refractive index related to the optical window has been shown in Fig. 7. Clearly, for the optical window as well, the refractive index distribution is non-uniform. When $t \leq 5$ s, due to the slow thermal evolution, the optical window is not heated considerably, and thus the refractive index changes insignificantly. However, when $t > 5$ s, the temperature of the window changes considerably, thus leading to a drastic change in the refractive index.

The irradiance received by the detector surface is shown in Fig. 8. After the optical head cover is heated to a high temperature, it will generate strong heat radiation. Due to its dependence on the temperature distribution of the optical window, the irradiance distribution received by the detector is not uniform. Furthermore, with the passage of working time, the radiation distribution received by the detector is almost constant, but the radiation illuminance value becomes increasingly larger. In addition, when $t < 5$ s, the radiation illuminance changes very little, whereas it increases rapidly for $t > 5$ s.

A. Simulation Results of the Wave Aberration

It should be noted that the exit pupil wave aberration results not only include the joint aero-optical transmission effects of the flow field and the optical window but also includes the aberration introduced by the optical window itself [29]. In order to more clearly clarify the influence of aero-optical effects on the imaging quality, the influence of the aberration of the optical window itself on the wave aberration should be removed. Hence, in this paper, the wave aberration of the pure optical window has been obtained first, as shown in Fig. 9. In particular, we compared the results obtained by the indigenously developed software with the results calculated by the traditional commercial software Zemax. A comparison of the results shows that the distribution of wave aberration results obtained by the two software packages is very similar. In addition, the values of the PV value of wavfront calculated by the indigenously developed software and the traditional software are 1.1262λ and 1.1272λ, respectively. The calculation error is below 0.09%, which verifies the reliability of the indigenously developed ray-tracing software.

The wave aberration for the joint influents for the aero-optical transmission effect of the flow field and the optical window in the working state has been calculated Fig. 10 illustrates the wave aberration resulting from the combined effect. The wave aberration on the exit pupil shows a non-uniform gradient distribution. Further, as the working time progresses, the gradient changes become increasingly obvious, and the peak wave aberration becomes increasingly larger. This shows that the imaging quality

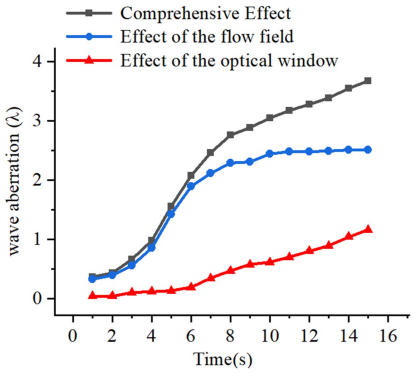

Fig. 11. The PV value of wavfront as a function under different aero-optical effects influences.

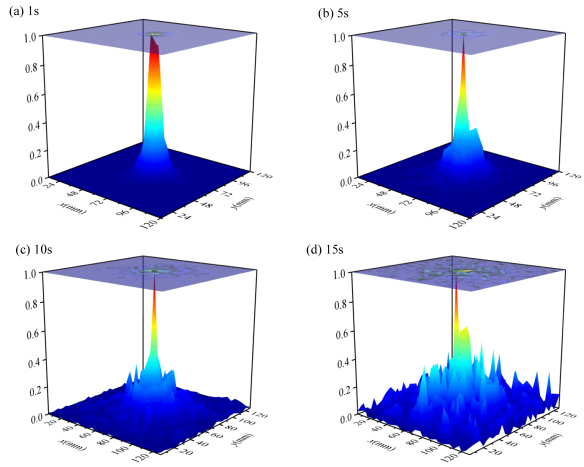

Fig. 12. The PSF simulation result obtained after aero-optical transmission in the simulation.

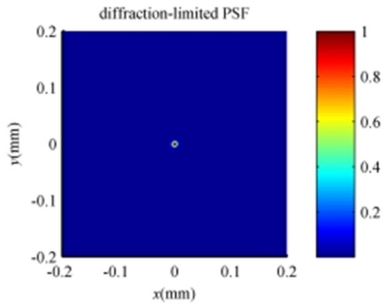

Fig. 13. The PSF of diffraction-limited.

of the infrared detection system worsens with a longer working time.

Affected by the aero-optical transmission effect, the PV and the RMS value of the wave aberration for the infrared detection system increases as the working time marching. The wave aberrations of the infrared detection system are compared before the aero-optical transmission effect occurs. Affected by the aero-optical transmission effect, the PV and RMS values of the wave aberration of the infrared detection system increase significantly, and this change becomes more obvious as time progresses. This shows that the aero-optical transmission effect does not correct the aberration introduced by the optical window itself but further degrades the imaging quality of the infrared detection system.

In order to clarify the influence of the aero-optical transmission effect of the flow field and the optical window separately, the wave aberration caused by the aero-optical transmission effect of the optical window was calculated. Further, by data processing, the changes in the PV value of wavfront as a function of the working time under different influences were plotted out, as shown in Fig. 11. It should be noted that data processing removes the aberration effect introduced by the optical window itself and only shows the impact on the optical effect. The flow field is obviously stronger than the optical window during aero-optical transmission effect on image quality. When the working time is $2 \leqslant t \leqslant 8$ s, the aero-optical transmission effect of flow field has the most serious impact on imaging. When $t \geqslant 8$ s, the influence of the optical window gradually manifested. PV value of wavfront

B. Simulation Results of the Point Spread Function

The PSF obtained after incorporating the effect of aero-optical transmission in the simulation has been shown in Fig. 12. With the advancement in the working hours of the infrared detection system, the radius of the dispersion radius of the PSF becomes increasingly larger, and an increasing number of "burrs" appear. This indicates that with the advancement of working hours, the image blur and offset caused by the pneumatic aero-optical transmission effect becomes increasingly serious.

In the diffraction-limited case, the radius of the dispersion spot should be infinitely small, as shown in Fig. 13.

We extracted the top view of the PSF as shown in Fig. 14. This can more intuitively show the change of PSF over time. When $t = 1$, the peak value of the point spread function is only one, but the dispersion radius increases significantly. With the progress of the working time, although the main peak of the point spread function can be distinguished, the secondary peaks gradually appear near it, and the number gradually increases. At the same time, the dispersion radius of the main peak increases accordingly.

C. Simulation Results of the Peak Signal-to-Noise Ratio

By performing a convolution calculation on the PSF, the final image caused by the aero-optical transmission effect was obtained from the infrared detection systems, as shown in Fig. 15. The prime minister's results are consistent with the previous analysis. With the increase in the working time, the effect of the pneumatic light transmission on imaging becomes increasingly serious, and the imaging quality gradually degrades.

Apart from the aero-optical transmission effect, the strategy developed in this study also considers aero-thermal radiation's effect on the imaging quality. Fig. 16 shows the joint influence of aero-optical transmission and aero-thermal radiation on the

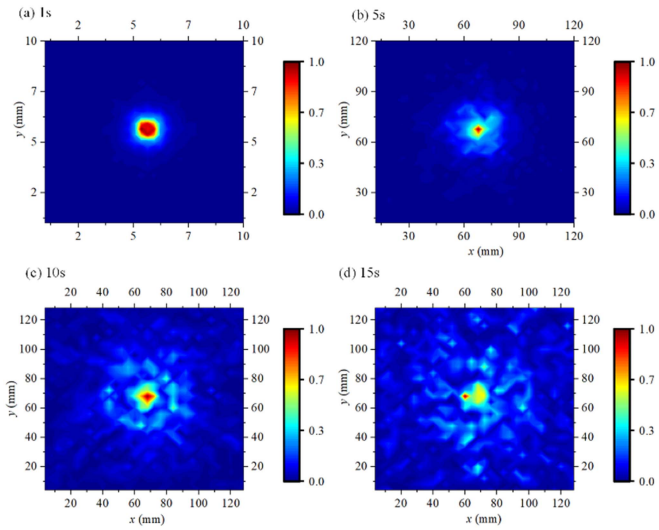

Fig. 14. The PSF simulation result obtained after aero-optical transmission in the simulation.

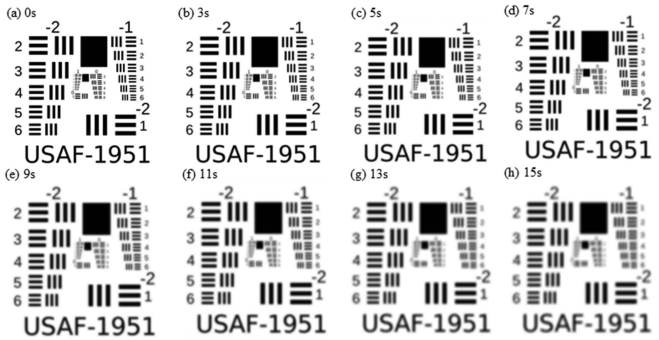

Fig. 15. Final image obtained from the infrared detection systems that is caused by the aero-optical transmission.

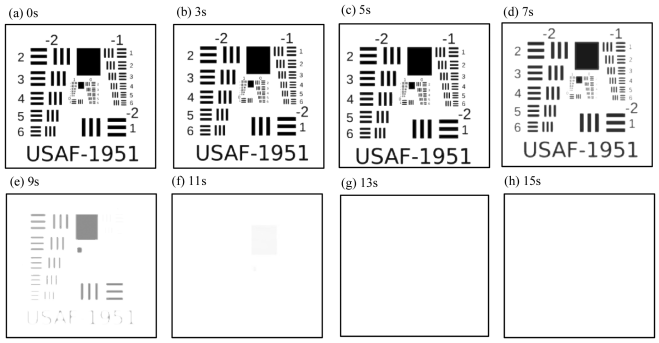

Fig. 16. Final image obtained from the infrared detection system that is caused by the joint influence of aero-optical transmission and the aero-thermal radiation.

imaging quality of an infrared detection system in its working state. The imaging results show that the aero-thermal radiation effect has a large impact on the imaging quality and cannot be ignored. When $t > 5$ s, the aero-thermal radiation effect is the main factor that determines the imaging quality. After $t > 11$ s, the infrared detection systems will be unable to track the target without any algorithmic processing accurately. The main reason

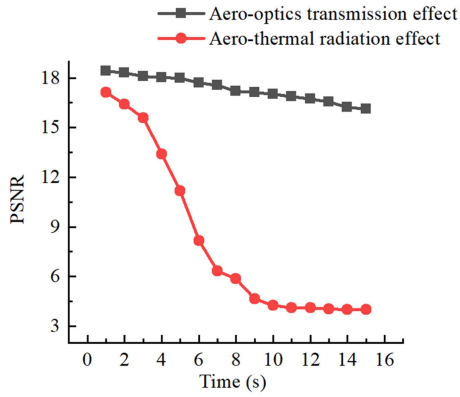

Fig. 17. The PSN simulation result.

for the rapid deterioration of the image quality at longer working times is the effect of the aero-thermal radiation.

For the influence of aero-optical effects on the background noise of the distorted image, the PSNR of the target image was obtained from simulation. The curve of the PSNR of the target image with time is shown in Fig. 17. In order to examine the influence of two kinds of aero-optical effects on images more intuitively, the PSNRs were obtained, respectively. The influence of the aero-thermal radiation effect on PSNR of the distorted image was obviously stronger compared with the aero-optical transmission effect. When the PSNR of the distorted image is reduced to remain unchanged, it indicates that the detector has reached saturation and the image information is overwhelmed by thermal radiation noise. When the working time is $t \geqslant 3$ s, PSNR decreases rapidly, and $t \geqslant 7$ s target signal information is gradually difficult to capture. When the working time is $t \geqslant 11$ s, the target signal cannot be distinguished.

V. Summary

In this study, the time characteristics of the degradation of the imaging quality of an infrared detection system resulting from the influence of the aero-optical effect on it have been explored. Three evaluation parameters, namely, wave aberration, PSF, and PSNR of the distorted images, were proposed to evaluate the infrared detection system's imaging quality. During the entire working process, the imaging quality of the infrared detector gradually deteriorated, and it mainly comes from the influence of aero-optical transmission and aero-thermal radiation effect. In the previous period of work, the image quality degradation of the aero-optical effect is not obvious, and the aero-optical transmission of the flow field is the main factor leading to the deterioration of the image quality. The aero-optical transmission effect of the flow field is the primary cause of the degraded image quality compared to the corresponding effect of the optical window. With time marching, the aero-thermal radiation effect will rapidly degrade the image quality. Even "thermal barrier" phenomenon gradually occurs, and the target signal is overwhelmed by the noise signal. The aero-thermal radiation effect is the most important reason for the obvious degradation of the imaging quality of the infrared detection system. The

time characteristic of the image quality deterioration hopefully provides a basis for the suppression of the aero-optical effect.

The results obtained in this study have limitations. The changing flight speed of the infrared detection system was considered, but the changing altitude was not discussed. This makes the research state deviate from the actual working state of the infrared detection system. The influence of height factors on aero-optical effects will be our future research direction.

ACKNOWLEDGMENT

The authors thank Dr. Sun for proofreading this paper; the authors are grateful to the reviewers and editors for their helpful and invaluable comments.

REFERENCES

[1] D. Wang, H. Luo, M. Li, and Y. Wang, "Research on simulation technology of infrared missile battle scene," *J. Phys.: Conf. Ser.*, vol. 1575, no. 1, 2020, Art. no. 012040.

[2] T. W. Rees, P. J. Bruce, T. B. Fisher, M. K. Quinn, and J. A. Merrifield, "Numerical and experimental studies of the hypersonic flow around a cube at incidence," *Acta Astronautica*, vol. 183, pp. 75–88, 2021.

[3] G. Guo, H. Liu, and B. Zhang, "Aero-optical effects of an optical seeker with a supersonic jet for hypersonic vehicles in near space," *Appl. Opt.*, vol. 55, no. 17, pp. 4741–4751, 2016.

[4] S. Chen, W. Zhang, C. Hao, B. Zuo, and Z. Fan, "Imaging quality evaluation of aerodynamically heated faceted dome based on ray tracing," *Optik-Int. J. Light Electron Opt.*, vol. 126, no. 19, pp. 1898–1904, 2015.

[5] J. Yu et al., "The suppression of aero-optical aberration of conformal dome by wavefront coding," *Opt. Commun.*, vol. 490, 2021, Art. no. 126876.

[6] W. Hui et al., "Evaluating imaging quality of optical dome affected by aero-optical transmission effect and aero-thermal radiation effect," *Opt. Exp.*, vol. 28, no. 5, pp. 6172–6187, 2020.

[7] T. Wang, Y. Zhao, D. Xu, and Q. Yang, "Numerical study of evaluating the optical quality of supersonic flow fields," *Appl. Opt.*, vol. 46, no. 23, pp. 5545–5551, 2007.

[8] Z. Wang, H. Xiao, Z. Fan, C. Qian, and C. Liu, "Radiation effect of aerodynamically heated optical dome on airborne infrared system," in *Proc. 8th Int. Symp. Precis. Eng. Meas. Instrum.*, 2013, vol. 8759, Art. no. 87593A.

[9] L. Liu, W. Meng, Y. Li, X. Dai, and Z. Zuo, "Influence of aero-optical transmission on infrared imaging optical system in the supersonic flight," *Infrared Phys. Technol.*, vol. 68, pp. 110–118, 2015.

[10] L. Xu, D. Xue, and X. Lv, "Computation and analysis of backward ray-tracing in aero-optics flow fields," *Opt. Exp.*, vol. 26, no. 1, pp. 567–576, 2018.

[11] L. Xu and Y. Cai, "Influence of altitude on aero-optic imaging deviation," *Appl. Opt.*, vol. 50, no. 18, pp. 2949–2957, 2011.

[12] S. Gordeyev, E. Jumper, and T. Hayden, "Aero-optical and hot-wire measurements of the flow around the hemispherical turret with a flat window," in *Proc. 35th AIAA Plasmadynamics Lasers Conf.*, 2004, Art. no. 2450.

[13] S. Gordeyev, T. E. Hayden, and E. J. Jumper, "Aero-optical and flow measurements over a flat-windowed turret," *AIAA J.*, vol. 45, no. 2, pp. 347–357, 2007.

[14] S. Gordeyev and E. Jumper, "Fluid dynamics and aero-optics of turrets," *Prog. Aerosp. Sci.*, vol. 46, no. 8, pp. 388–400, 2010.

[15] H. Xiao and Z. Fan, "Imaging quality evaluation of aerodynamically heated optical dome using ray tracing," *Appl. Opt.*, vol. 49, no. 27, pp. 5049–5058, 2010.

[16] H. Xiao, Z. Wang, and Z. Fan, "Optical distortion evaluation of an aerodynamically heated window using the interfacial fluid thickness concept," *Appl. Opt.*, vol. 50, no. 19, pp. 3135–3144, 2011.

[17] C. Hao et al., "Comprehensive analysis of imaging quality degradation of an airborne optical system for aerodynamic flow field around the optical window," *Appl. Opt.*, vol. 52, no. 33, pp. 7889–7898, 2013.

[18] C. M. Ostoich, D. J. Bodony, and P. H. Geubelle, "Fluid-thermal response of spherical dome under a mach 6.59 laminar boundary layer," *AIAA J.*, vol. 50, pp. 2791–2808, 2012.

[19] A. J. Culler and J. J. McNamara, "Impact of fluid-thermal-structural coupling on response prediction of hypersonic skin panels," *AIAA J.*, vol. 49, pp. 2393–2406, 2011.

[20] C. Farhat and P. Geuzaine, "Design and analysis of robust ALE time-integrators for the solution of unsteady flow problems on moving grids," *Comput. Methods Appl. Mechanics Eng.*, vol. 193, pp. 4073–4095, 2004.

[21] R. E. Bartels, "Mesh strategies for accurate computation of unsteady spoiler and aeroelastic problems," *J. Aircr.*, vol. 37, pp. 521–525, 2000.

[22] P. Geuzaine, C. Grandmont, and C. Farhat, "Design and analysis of ALE schemes with provable second-order time-accuracy for inviscid and viscous flow simulations," *J. Comput. Phys.*, vol. 191, pp. 206–227, 2003.

[23] C. Farhat, K. G. Van der Zee, and P. Geuzaine, "Provably second-order time-accurate loosely-coupled solution algorithms for transient nonlinear computational aeroelasticity," *Comput. Methods Appl. Mechanics Eng.*, vol. 195, pp. 1973–2001, 2006.

[24] A. R. Crowell, B. A. Miller, and J. J. McNamara, "Robust and efficient treatment of temperature feedback in fluid–thermal–structural analysis," *AIAA J.*, vol. 52, pp. 2395–2413, 2014.

[25] B. A. Miller and J. J. McNamara, "Time-marching considerations for response prediction of structures in hypersonic flows," *AIAA J.*, vol. 53, pp. 3028–3038, 2015.

[26] J. N. Reddy, *An Introduction to Nonlinear Finite Element Analysis*. Oxford, U.K.: Oxford Univ., 2004.

[27] H. Wang et al., "Influence of altitude on aero-optic imaging quality degradation of the hemispherical optical dome," *Appl. Opt.*, vol. 58, no. 2, pp. 274–282, 2019.

[28] A. Hore and D. Ziou, "Image quality metrics: PSNR vs. SSIM," in *Proc. 20th Int. Conf. Pattern Recognit.*, 2010, pp. 2366–2369.

[29] F. Dang et al., "Basic geometry and aberration characteristics of conicoidal conformal domes," *Appl. Opt.*, vol. 55, no. 31, pp. 8713–8721, 2016.